Geophysical Prospecting, 2006, **54**, 535–552

Non-hyperbolic moveout inversion of wide-azimuth P-wave data for orthorhombic media

Ivan Vasconcelos* and Ilya Tsvankin

Center for Wave Phenomena, Department of Geophysics, Colorado School of Mines, Golden, CO 80401-1887, USA

Received February 2005, revision accepted January 2006

ABSTRACT

The azimuthally varying non-hyperbolic moveout of P-waves in orthorhombic media can provide valuable information for characterization of fractured reservoirs and seismic processing. Here, we present a technique to invert long-spread, wide-azimuth P-wave data for the orientation of the vertical symmetry planes and five key moveout parameters: the symmetry-plane NMO velocities, $V_{\rm nmo}^{(1)}$ and $V_{\rm nmo}^{(2)}$, and the anellipticity parameters, $\eta^{(1)}$, $\eta^{(2)}$ and $\eta^{(3)}$. The inversion algorithm is based on a coherence operator that computes the semblance for the full range of offsets and azimuths using a generalized version of the Alkhalifah–Tsvankin non-hyperbolic moveout equation.

The moveout equation provides a close approximation to the reflection traveltimes in layered anisotropic media with a uniform orientation of the vertical symmetry planes. Numerical tests on noise-contaminated data for a single orthorhombic layer show that the best-constrained parameters are the azimuth φ of one of the symmetry planes and the velocities $V_{\rm nmo}^{(1)}$ and $V_{\rm nmo}^{(2)}$, while the resolution in $\eta^{(1)}$ and $\eta^{(2)}$ is somewhat compromised by the trade-off between the quadratic and quartic moveout terms. The largest uncertainty is observed in the parameter $\eta^{(3)}$, which influences only long-spread moveout in off-symmetry directions. For stratified orthorhombic models with *depth-dependent* symmetry-plane azimuths, the moveout equation has to be modified by allowing the orientation of the effective NMO ellipse to differ from the principal azimuthal direction of the effective quartic moveout term.

The algorithm was successfully tested on wide-azimuth P-wave reflections recorded at the Weyburn Field in Canada. Taking azimuthal anisotropy into account increased the semblance values for most long-offset reflection events in the overburden, which indicates that fracturing is not limited to the reservoir level. The inverted symmetry-plane directions are close to the azimuths of the off-trend fracture sets determined from borehole data and shear-wave splitting analysis. The effective moveout parameters estimated by our algorithm provide input for P-wave time imaging and geometrical-spreading correction in layered orthorhombic media.

INTRODUCTION

Non-hyperbolic (long-spread) moveout is often used in velocity analysis of P-waves in transversely isotropic media with a vertical symmetry axis (VTI). All P-wave time-domain signatures in VTI models with a laterally homogeneous overburden above the horizon of interest depend on just two interval parameters, i.e. the normal-moveout (NMO) velocity from a horizontal reflector ($V_{\rm nmo}$) and the 'anellipticity' coefficient η (Alkhalifah and Tsvankin 1995; Tsvankin 2005). The velocity $V_{\rm nmo}$ controls conventional-spread traveltimes of horizontal P-wave events, while η is responsible for the non-hyperbolic moveout at long offsets. Most implementations of

*E-mail: ivascon@dix.mines.edu

non-hyperbolic moveout inversion for VTI media (e.g. Alkhalifah 1997; Toldi *et al.* 1999) are based on the moveout equation of Tsvankin and Thomsen (1994) represented in terms of V_{nmo} and η by Alkhalifah and Tsvankin (1995).

The model-independent form of the original Tsvankin–Thomsen (1994) equation makes it suitable for the more complicated azimuthally anisotropic media, typically associated with natural fractures or TI layers with a tilted symmetry axis. (Note that an alternative description of non-hyperbolic moveout in azimuthally anisotropic media was suggested by Sayers and Ebrom (1997), who devised a formalism based on spherical harmonics.) The key parameters of the equation are the NMO velocity and the quartic moveout coefficient A_4, both dependent on the source-to-receiver azimuth. Even for azimuthally anisotropic and laterally heterogeneous media, the NMO velocity as a function of azimuth is described by a simple quadratic form and usually traces out an ellipse in the horizontal plane (Grechka and Tsvankin 1998a). The quartic coefficient A_4 for horizontally-layered HTI (TI with a horizontal symmetry axis) and orthorhombic media was derived by Al-Dajani and Tsvankin (1998) and Al-Dajani *et al.* (1998), who also showed that the Tsvankin–Thomsen equation remains accurate even in the presence of pronounced azimuthal anisotropy. Pech, Tsvankin and Grechka (2003) gave a more general analytic description of A_4, valid for arbitrary anisotropy and heterogeneity, that was applied by Pech and Tsvankin (2004) to P-wave non-hyperbolic moveout in dipping orthorhombic layers.

The goal of this paper is to develop a practical methodology to invert P-wave non-hyperbolic moveout for horizontally layered orthorhombic models. Although treatment of the simpler HTI medium is much more straightforward, it is believed that realistic models of fractured reservoirs have orthorhombic or even lower symmetry (Schoenberg and Helbig 1997; Bakulin *et al.* 2000). In principle, useful information for fracture characterization can be obtained from NMO ellipses alone, without employing reflection traveltime at long offsets (Bakulin *et al.* 2000; Jenner 2001; Grechka, Pech and Tsvankin 2002). The inversion of NMO ellipses, however, is often ambiguous and requires *a priori* constraints on the symmetry and some of the model parameters, in particular when only P-wave data are available (Grechka and Tsvankin 1999a; Bakulin *et al.* 2000).

Non-hyperbolic moveout of P-waves in orthorhombic media is governed by the azimuth of one of the vertical symmetry planes, the NMO velocities ($V_{\mathrm{nmo}}^{(1)}$ and $V_{\mathrm{nmo}}^{(2)}$) in the symmetry-plane directions, and three anisotropic 'anellipticity' coefficients $\eta^{(1,2,3)}$ (Al-Dajani *et al.* 1998). Since both the ratio of the symmetry-plane NMO velocities and coefficients $\eta^{(1,2,3)}$ for fracture-induced orthorhombic models are sensitive to the fracture compliances and orientations (Bakulin *et al.* 2000), non-hyperbolic moveout inversion can help in building more accurate physical models for reservoir characterization. As shown by Grechka and Tsvankin (1999b), the parameters $V_{\mathrm{nmo}}^{(1,2)}$ and $\eta^{(1,2,3)}$ are responsible for all time-processing steps for orthorhombic anisotropy, including NMO and dip-moveout (DMO) corrections, and pre-stack and post-stack time migration. Therefore, the moveout parameters estimated from long-spread moveout can also be used in imaging P-wave data from orthorhombic formations.

A particularly convenient P-wave moveout approximation for an orthorhombic layer, which has the same form as the Alkhalifah–Tsvankin (1995) non-hyperbolic equation for VTI media, was suggested by Xu, Tsvankin and Pech (2005). Here, we use the equation of Xu *et al.* (2003) to invert for the orientation of the symmetry planes and five moveout parameters from 3D wide-azimuth, long-spread data. Our method represents an extension to non-hyperbolic moveout of the 3D semblance technique devised by Grechka and Tsvankin (1999a) for the estimation of NMO ellipses. To account for possible misalignment of the vertical symmetry planes in a stack of orthorhombic layers, the principal azimuthal directions of the quartic moveout coefficient should be decoupled from the NMO ellipse. After describing the inversion algorithm and testing it on synthetic data, we apply non-hyperbolic moveout analysis to field data acquired over a fractured reservoir at the Weyburn Field in Canada.

NON-HYPERBOLIC MOVEOUT IN ORTHORHOMBIC MEDIA

Models of orthorhombic symmetry are commonly used to describe naturally fractured formations (e.g. Schoenberg and Helbig 1997; Bakulin *et al.* 2000). Orthorhombic media have three mutually orthogonal symmetry planes, one of which we assume to be horizontal (Fig. 1). Kinematic signatures and plane-wave polarizations of P- and S-waves in the symmetry planes can be described by the same equations as in VTI media. This equivalence between VTI and the symmetry planes of orthorhombic media was used by Tsvankin (1997, 2005) to introduce Thomsen-style notation for orthorhombic models (see Appendix).

The non-hyperbolic moveout equation of Tsvankin and Thomsen (1994), which was originally designed for layer-cake VTI media, remains valid in both vertical symmetry planes of an orthorhombic layer. Al-Dajani *et al.* (1998) demonstrated

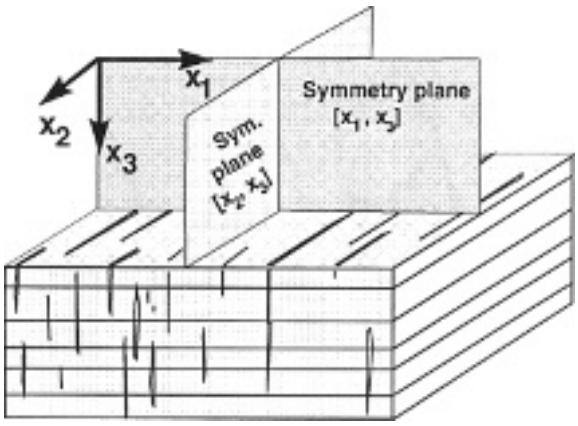

Figure 1 Orthorhombic models are characterized by three mutually orthogonal planes of mirror symmetry. Effective orthorhombic anisotropy may be caused by parallel, vertical, penny-shaped cracks embedded in a VTI matrix.

that the Tsvankin–Thomsen equation can be applied in off-symmetry directions as well by making the moveout coefficients, A_2, A_4 and A, azimuthally dependent:

$$t^2(x,\alpha) = A_0 + A_2(\alpha)\,x^2 + \frac{A_4(\alpha)\,x^4}{1 + A(\alpha)\,x^2}\,, \tag{1}$$

$$A_0 = t_0^2\,, \tag{2}$$

$$A_2(\alpha) = \left.\frac{\mathrm{d}(t^2)}{\mathrm{d}(x^2)}\right|_{x=0}\,, \tag{3}$$

$$A_4(\alpha) = \frac{1}{2}\,\frac{\mathrm{d}}{\mathrm{d}(x^2)}\,\left.\frac{\mathrm{d}(t^2)}{\mathrm{d}(x^2)}\right|_{x=0}\,. \tag{4}$$

Here, t is the reflection traveltime, x is the source–receiver offset, α is the azimuth with respect to the $[x_1, x_3]$ symmetry plane, t_0 is the zero-offset time, A_2 controls the hyperbolic portion of the moveout curve, and A_4 is the quartic moveout coefficient that accounts for non-hyperbolic moveout at long offsets. The parameter A was introduced by Tsvankin and Thomsen (1994) to make $t(x)$ convergent for $x \to \infty$:

$$A(\alpha) = \frac{A_4(\alpha)}{V_{\mathrm{hor}}^{-2}(\alpha) - V_{\mathrm{nmo}}^{-2}(\alpha)}\,, \tag{5}$$

where V_{hor} is the horizontal group velocity.

The quadratic moveout coefficient $A_2(\alpha) = 1/V_{\mathrm{nmo}}^2(\alpha)$ depends on the azimuthally-varying NMO velocity $V_{\mathrm{nmo}}(\alpha)$ that typically traces out an ellipse (Grechka and Tsvankin 1998a). In a single horizontal orthorhombic layer, the axes of the NMO ellipse are aligned with the vertical symmetry planes:

$$A_2(\alpha) = A_2^{(1)}\sin^2\alpha + A_2^{(2)}\cos^2\alpha\,, \tag{6}$$

where

$$A_2^{(1)} = \frac{1}{[V_{\mathrm{nmo}}^{(1)}]^2}\,, \quad A_2^{(2)} = \frac{1}{[V_{\mathrm{nmo}}^{(2)}]^2}\,, \tag{7}$$

and $V_{\mathrm{nmo}}^{(1)}$ and $V_{\mathrm{nmo}}^{(2)}$ are the NMO velocities in the symmetry planes $[x_2, x_3]$ and $[x_1, x_3]$, respectively (the superscript denotes the axis orthogonal to the plane; see Appendix for details).

Al-Dajani *et al.* (1998) showed that the azimuthal dependence of the quartic moveout coefficient A_4 in an orthorhombic layer has the following form:

$$A_4(\alpha) = A_4^{(1)}\sin^4\alpha + A_4^{(2)}\cos^4\alpha + A_4^{(x)}\sin^2\alpha\,\cos^2\alpha\,. \tag{8}$$

The coefficients $A_4^{(1)}$ and $A_4^{(2)}$ control non-hyperbolic moveout in the symmetry planes, while $A_4^{(x)}$ is a cross-term that contributes to long-offset traveltimes in off-symmetry azimuthal directions. All three coefficients in (8) can be expressed through the symmetry-plane NMO velocities and the anellipticity parameters $\eta^{(1,2,3)}$ defined in the Appendix. Substitution of (8) and (6) into the moveout equation (1) yields a close approximation for P-wave reflection traveltimes up to offset-to-depth ratios of about three (Al-Dajani *et al.* 1998).

For purposes of moveout inversion, it is more convenient to use a simplified form of the general equation (1) based on the approximate kinematic equivalence between vertical planes of orthorhombic and VTI media (Xu *et al.* 2005). Kinematic signatures and plane-wave polarizations in the symmetry planes of orthorhombic models can be described by the corresponding VTI equations (e.g. Tsvankin 1997, 2005). This equivalence with VTI media is no longer exact in vertical off-symmetry planes, but it remains valid for 2D P-wave kinematics in the weak-anisotropy approximation. P-wave phase velocity and all other 2D kinematic signatures in any vertical plane of weakly anisotropic orthorhombic media can be adapted from the VTI equations by using azimuthally-dependent Thomsen parameters ϵ and δ (Tsvankin 1997, 2005). Therefore, the widely used non-hyperbolic moveout equation for VTI media in terms of the velocity V_{nmo} and parameter η (Alkhalifah and Tsvankin 1995; Tsvankin 2005) can be applied to orthorhombic media by making both parameters functions of azimuth (Xu *et al.* 2005):

$$t^2(x) = t_0^2 + \frac{x^2}{V_{\mathrm{nmo}}^2(\alpha)} - \frac{2\eta(\alpha)\,x^4}{V_{\mathrm{nmo}}^2(\alpha)\,[t_0^2\,V_{\mathrm{nmo}}^2(\alpha) + (1+2\eta(\alpha))\,x^2]}\,, \tag{9}$$

$$V_{\mathrm{nmo}}^{-2}(\alpha) = \frac{\sin^2(\alpha-\varphi)}{[V_{\mathrm{nmo}}^{(1)}]^2} + \frac{\cos^2(\alpha-\varphi)}{[V_{\mathrm{nmo}}^{(2)}]^2}\,, \tag{10}$$

$$\eta(\alpha) = \eta^{(2)}\cos^2(\alpha-\varphi) - \eta^{(3)}\cos^2(\alpha-\varphi)\,\sin^2(\alpha-\varphi) + \eta^{(1)}\sin^2(\alpha-\varphi)\,, \tag{11}$$

where α is the source-to-receiver azimuth with respect to the acquisition frame, and φ is the azimuth of the $[x_1, x_3]$ symmetry plane of the orthorhombic medium. Equation (11) for the parameter $\eta(\alpha)$ was obtained by Pech and Tsvankin (2004); it also follows from the results of Tsvankin (1997).

Note that although the equivalence between orthorhombic and VTI media for off-symmetry azimuths is strictly valid only for weak orthorhombic anisotropy, the original Alkhalifah–Tsvankin (1995) equation is not a weak-anisotropy approximation. The results of Xu *et al.* (2005) and the numerical testing below show that (9) is sufficiently accurate for a wide range of moderately anisotropic orthorhombic models typical for fractured reservoirs. In principle, the approach described here can be used to extend other existing VTI moveout approximations (Fomel 2004; Stovas and Ursin 2004; van der Baan 2004; Douma and Calvert 2006) to orthorhombic media. These approximations, however, are either limited to a single layer (Fomel 2004) or provide tangible gains in accuracy compared to the Alkhalifah–Tsvankin equation only for large values of $\eta > 0.25$ (e.g. Douma and Calvert 2006). Since for such strongly anelliptical models the equivalence between VTI and orthorhombic symmetry can break down, it remains to be seen if the advantages of these VTI equations can be preserved for azimuthally anisotropic media.

In the vertical symmetry plane $[x_1, x_3]$ ($\alpha = \varphi$), equation (9) reduces to the moveout equation for VTI media parametrized by $V^{(2)}_{\rm nmo}$ and $\eta^{(2)}$, while for the plane $[x_2, x_3]$ ($\alpha = \varphi \pm 90^\circ$), the parameters are $V^{(1)}_{\rm nmo}$ and $\eta^{(1)}$. The accuracy of (9) in both symmetry planes is the same as that in the corresponding VTI medium and can be assessed using the results of Grechka and Tsvankin (1998b) and Tsvankin (2005). Although (9) is strictly valid only in weakly anisotropic media, Xu *et al.* (2005) showed that it provides a good approximation for reflection traveltimes even for substantial variations in P-wave velocity.

However, the analysis of Xu *et al.* (2005) was limited to a single horizontal orthorhombic layer. To be effective in field-data applications, the moveout equation has to provide sufficient accuracy for stratified models that can include orthorhombic and HTI layers with different orientations of the vertical symmetry planes. The main complications caused by the absence of a uniform symmetry-plane direction include additional terms in the azimuthal variation of the quartic moveout coefficient A_4 (Al-Dajani *et al.* 1998) and the possible misalignment of the NMO ellipse with the 'principal axes' of A_4. Here, we follow the approach of Xu and Tsvankin (2004), who suggested modifying (11) by introducing a separate azimuthal angle φ_1 responsible for the azimuthal variation of A_4 and the effective parameter $\eta(\alpha)$:

$$\eta(\alpha) = \eta^{(2)}\cos^2(\alpha-\varphi_1) - \eta^{(3)}\cos^2(\alpha-\varphi_1)\,\sin^2(\alpha-\varphi_1) + \eta^{(1)}\sin^2(\alpha-\varphi_1)\,. \tag{12}$$

Below, we study the accuracy of (9) for layered azimuthally anisotropic media using two different forms of the effective parameter $\eta(\alpha)$ [equations (11) and (12)].

INVERSION ALGORITHM

Our parameter-estimation algorithm is designed to estimate the azimuth φ (and possibly φ_1) and the parameters $V^{(1)}_{\rm nmo}$, $V^{(2)}_{\rm nmo}$, $\eta^{(1)}$, $\eta^{(2)}$ and $\eta^{(3)}$ using the moveout equation (9). The parameter $\eta(\alpha)$ is described by either (11) or (12), depending on whether or not the model has misaligned symmetry planes. Non-hyperbolic moveout inversion in orthorhombic media requires long-spread P-wave data to be recorded for a wide range of azimuths. Whereas the NMO ellipse can be reconstructed using just three differently orientated lines (Grechka and Tsvankin 1998a), the inversion for the η parameters is less stable (see below) and cannot be accomplished without a much more complete azimuthal coverage.

One possible way of processing wide-azimuth data is to divide the traces in each superbin (or supergather) into azimuthal sectors with a certain increment in azimuth (e.g. 10°) and perform the moveout inversion for the local values of $V_{\rm nmo}(\alpha)$ and $\eta(\alpha)$ in each sector separately. The VTI models obtained for all sectors can then be combined into a best-fit orthorhombic model. The azimuthal sectoring, however, can introduce bias into the velocity analysis because the data sampling in offset and azimuth is never uniform, and the inversion results can depend on the number and size of the sectors (Grechka and Tsvankin 1999a). Also, combining traces with different azimuths into the same sector can be particularly harmful for non-hyperbolic moveout inversion because traveltime variations with azimuth are more pronounced at long offsets.

Here, we follow the approach of Grechka and Tsvankin (1999a), who suggested processing all traces for a given superbin simultaneously, using a 3D semblance operator. However, while the work of Grechka and Tsvankin (1999a) is limited to the estimation of NMO ellipses from the hyperbolic moveout on conventional-length spreads, we employ the full range of available offsets (from $x_{\rm min}$ to $x_{\rm max}$)

and azimuths (from $\alpha_{\min}$ to $\alpha_{\max}$). The 3D semblance (objective) function to be maximized for each zero-offset reflection time t_0 is given by (for media with aligned symmetry planes)

$$S(t_0, V_{\rm nmo}^{(1)}, V_{\rm nmo}^{(2)}, \eta^{(1)}, \eta^{(2)}, \eta^{(3)}, \varphi) = \frac{\sum_{t_0-T/2}^{t_0+T/2}[\sum_{x_{\min}}^{x_{\max}} \sum_{\alpha_{\min}}^{\alpha_{\max}} U(x, \alpha, t)]^2}{\sum_{t_0-T/2}^{t_0+T/2} \sum_{x_{\min}}^{x_{\max}} \sum_{\alpha_{\min}}^{\alpha_{\max}} U^2(x, \alpha, t)}, \quad (13)$$

where U is the measured amplitude, and the semblance is calculated for the time window T around the reflection time t obtained from (9).

To aid the efficiency of the algorithm, we precede the full 3D semblance search for the best-fit model by two preliminary parameter-estimation steps designed to find approximate values of all model parameters except $\eta^{(3)}$. Firstly, we mute out long offsets and apply the algorithm of Grechka and Tsvankin (1999a) to reconstruct the best-fit NMO ellipse for each reflection event. The orientation and semi-axes of the NMO ellipse yield the initial values for the symmetry-plane orientation (angle φ) and velocities $V_{\rm nmo}^{(1)}$ and $V_{\rm nmo}^{(2)}$. Secondly, we perform 2D non-hyperbolic moveout inversion in two narrow azimuthal sectors aligned with the identified symmetry-plane directions to estimate the parameters $\eta^{(1)}$ and $\eta^{(2)}$, which govern long-spread moveout in the planes $[x_2, x_3]$ and $[x_1, x_3]$, respectively.

For azimuthally anisotropic models with a uniform orientation of the vertical symmetry planes, the two preliminary steps usually produce an initial model that is close (except for the parameter $\eta^{(3)}$) to the final best-fit model. Finally, we apply the Powell method (Press *et al.* 1987) to maximize semblance and thus invert for all six parameters using the full range of offsets and azimuths. Since the search does not start far from the maximum of the objective function, the algorithm usually converges in less than 20 iterations. If the model includes layers with depth-varying azimuths of the symmetry planes, the only change in the inversion methodology described above is that the 3D semblance search is carried out using (12) for $\eta(\alpha)$ instead of (11). During this search, we estimate the azimuth φ_1, while holding the orientation of the NMO ellipse (i.e. the azimuth φ) constant.

TESTS ON SYNTHETIC DATA

The synthetic examples below help us to assess whether the inversion is sufficiently robust in the presence of random noise and can provide an accurate estimate of the medium parameters starting from different initial solutions in the model space. It is also important to evaluate the performance of the algorithm for layered media that do not conform to the model assumptions that underlie (9), originally derived for a homogeneous orthorhombic layer.

Single orthorhombic layer

The first test (Fig. 2) is performed for a single horizontal layer using full-azimuth, long-offset P-wave synthetic data generated by anisotropic ray tracing (Gajewski and Pšenčík 1987). Following the methodology described above, we start by estimating the NMO ellipse using source–receiver pairs with offset-to-depth ratios up to one, which gives initial values for the symmetry-plane azimuth $\varphi = 130^\circ$, and the velocities $V_{\rm nmo}^{(1)} = 2345$ m/s and $V_{\rm nmo}^{(2)} = 2715$ m/s (the model parameters are listed in the caption of Fig. 2). The high semblance value (0.97) and the accurate estimate of φ confirm that the reconstructed NMO ellipse provides a good fit to conventional-spread data. The deviations of the symmetry-plane NMO velocities from the actual values are caused by the small influence of non-hyperbolic moveout unaccounted for at this stage of the inversion.

Next, we form two azimuthal sectors, 10° wide, around the identified symmetry-plane directions and carry out 2D non-hyperbolic moveout analysis in these sectors (i.e. we apply the VTI inversion) to obtain approximate values of $\eta^{(1)}$ and $\eta^{(2)}$. The results are shown in Fig. 2 as functions of $V_{\rm nmo}$ and the horizontal velocity $V_{\rm hor} = V_{\rm nmo}\sqrt{1+2\eta}$ related to the corresponding η coefficient. The errors in both η parameters are caused by a slight bias in the 2D non-hyperbolic moveout equation and by the azimuthal variations in traveltimes within both azimuthal sectors. Using these initial values, we carry out the 3D non-hyperbolic moveout inversion for the whole data set and obtain the following estimates of the model parameters: $\varphi = 130^\circ$, $V_{\rm nmo}^{(1)} = 2277$ m/s, $V_{\rm nmo}^{(2)} = 2703$ m/s, $\eta^{(1)} = 0.18$, $\eta^{(2)} = 0.06$ and $\eta^{(3)} = 0.11$; the semblance for the best-fit model is 0.89.

Figure 3 demonstrates that the bias of our 3D methodology in estimating the parameters $V_{\rm nmo}^{(1)}$, $V_{\rm nmo}^{(2)}$, $\eta^{(1)}$ and $\eta^{(2)}$ is close to that in the 2D (VTI) non-hyperbolic moveout inversion of Alkhalifah (1997) and Grechka and Tsvankin (1998b). Grechka and Tsvankin (1998b) and Tsvankin (2005) discussed this bias, which is caused by the design of the moveout equation. We processed the data from the model in Fig. 2 to find the best-fit values of $V_{\rm nmo}^{(1)}$ and $\eta^{(1)}$ using both the 3D and 2D algorithms (Fig. 3); the 2D (VTI) equation was applied to the data in the $[x_2, x_3]$-plane. The optimization procedure was

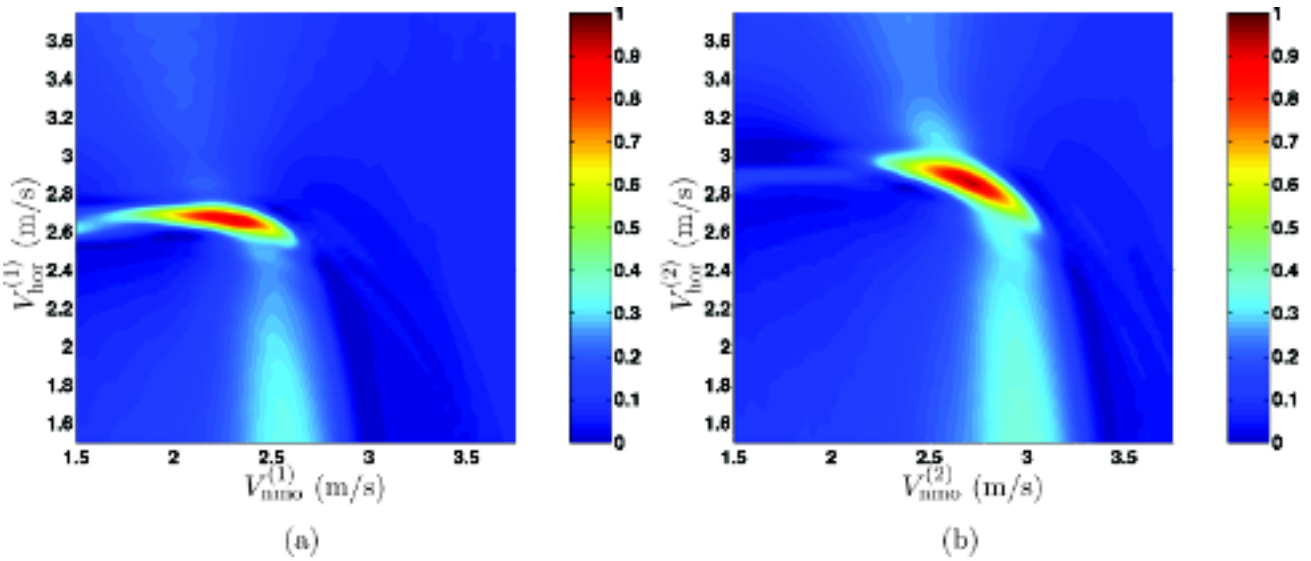

Figure 2 Results of a synthetic test on P-wave data computed by anisotropic ray tracing for a horizontal orthorhombic layer. The plots show semblance contours obtained by scanning over $V_{\rm nmo}$ and $V_{\rm hor}$ (i.e. by applying the VTI moveout-inversion algorithm) in the azimuthal sectors centred at the vertical symmetry planes identified from the NMO ellipse. The maximum offset-to-depth ratio is three. (a) The sector around the $[x_2, x_3]$ symmetry plane at $\varphi = 40^\circ$ (derived estimate $\eta^{(1)} = 0.178$); (b) the sector around the $[x_1, x_3]$ symmetry plane at $\varphi = 130^\circ$ (derived estimate $\eta^{(2)} = 0.05$). The true model parameters are $\varphi = 130^\circ$, $V_{\rm nmo}^{(1)} = 2269$ m/s, $V_{\rm nmo}^{(2)} = 2699$ m/s, $\eta^{(1)} = 0.196$, $\eta^{(2)} = 0.065$ and $\eta^{(3)} = 0.094$.

carried out for a large number of randomly chosen starting models to sample the ranges of both inverted parameters.

For all maximum offset-to-depth ratios ($x/z = 2$, 3, 4) used in Fig. 3, the bias in the 3D and 2D estimates of $V_{\rm nmo}^{(1)}$ and $\eta^{(1)}$ is comparable. When $x/z = 2$ (Fig. 3a), both algorithms underestimate the value of $\eta^{(1)}$ by about 0.025, which is consistent with the results of Grechka and Tsvankin (1998b). This small bias in η tends to decrease for larger spread-lengths, whereas the bias in $V_{\rm nmo}$ increases but for $x/z < 4$ remains within the limit of about 1% (Fig. 3b,c).

Although the algorithm in this noise-free test was able to converge toward the correct model, it is important to identify possible trade-offs among the medium parameters by studying the shape of the objective function. To display such trade-offs, we hold four model parameters at the correct values and compute the objective function near the actual solution as a function of the remaining two parameters. Figure 4 shows the semblance scan over the parameters $V_{\rm nmo}^{(2)}$ and $\eta^{(2)}$ computed from (9) using the correct values of φ, $V_{\rm nmo}^{(1)}$, $\eta^{(1)}$ and $\eta^{(3)}$. Clearly, there exists a family of models with a relatively wide range of $\eta^{(2)}$ values that fit the data, whereas the velocity $V_{\rm nmo}^{(2)}$ is constrained much more tightly.

This trade-off between $V_{\rm nmo}^{(2)}$ and $\eta^{(2)}$ has the same character as the interplay between the NMO velocity and η in VTI media (Alkhalifah 1997; Grechka and Tsvankin 1998b; Tsvankin 2005). Relatively small percentage errors in $V_{\rm nmo}^{(2)}$ can be compensated by larger absolute errors in $\eta^{(2)}$ in such a way that the reflection traveltime stays almost the same. The ambiguity in $\eta^{(2)}$ can be substantially reduced by increasing the maximum offset-to-depth ratio x/z from two (Fig. 4a) to three (Fig. 4c).

Large offset-to-depth ratios are also necessary to estimate the other two anellipticity coefficients, $\eta^{(1)}$ and $\eta^{(3)}$, which contribute only to non-hyperbolic moveout on long spreads. However, since the parameter $\eta^{(3)}$ has no influence on reflection traveltimes near either symmetry plane, it is constrained more poorly than $\eta^{(1)}$ and $\eta^{(2)}$ (Fig. 5a). In contrast, the inversion algorithm yields a highly accurate estimate of the azimuth φ (Fig. 5b) because the orientation of the symmetry planes can be inferred from both the NMO ellipse and azimuthally varying non-hyperbolic moveout.

Figure 6 confirms that the inversion results for $\eta^{(3)}$, as well as for the other parameters (not shown), are not sensitive to random (Gaussian) noise. The signal-to-noise ratio (S/N) in this test is defined as the ratio of the maximum absolute amplitudes of the signal and noise on each trace. The stability of the parameter estimation in the presence of random noise is not surprising because our algorithm is based on the semblance (coherence) operator (13).

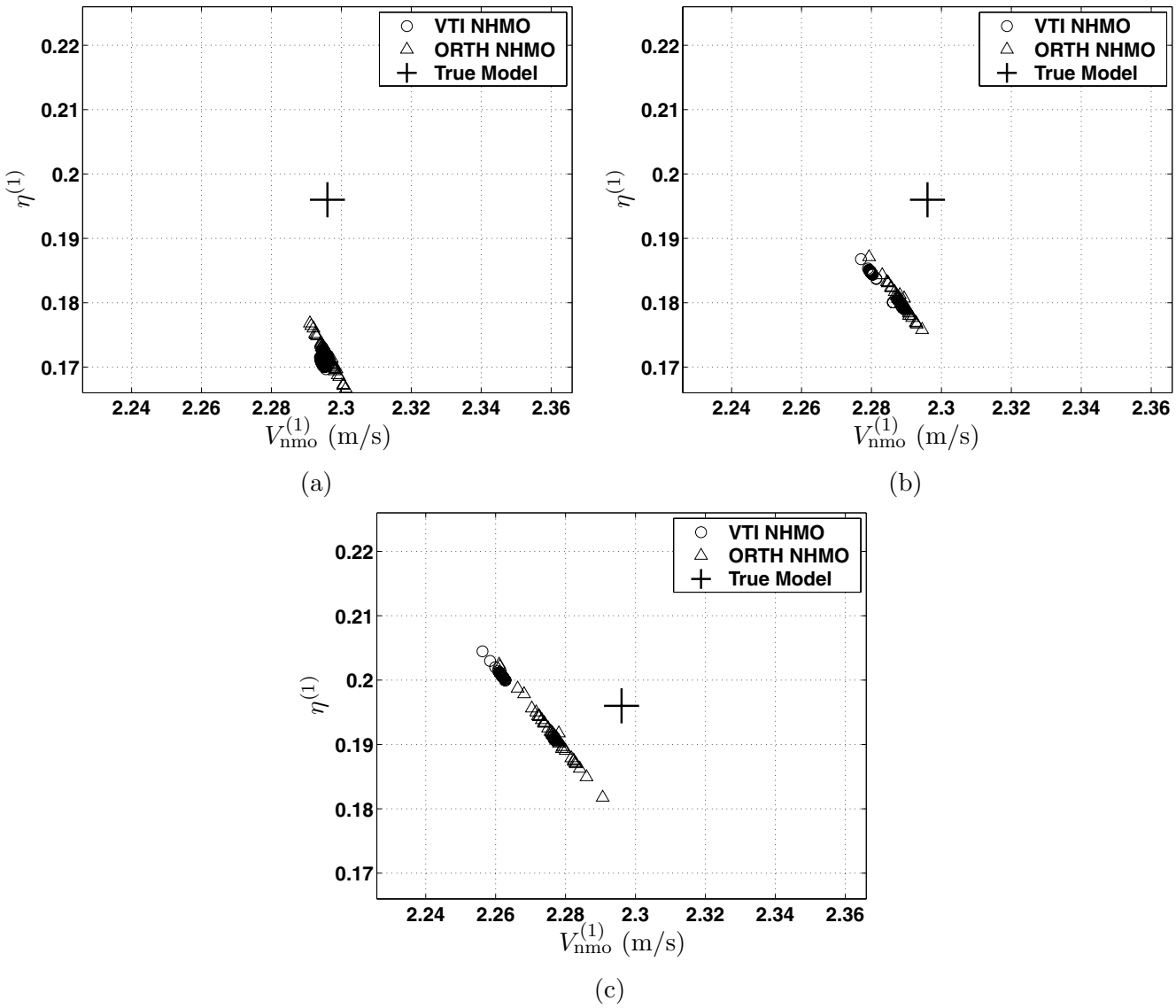

Figure 3 Parameters $V^{(1)}_{\rm nmo}$ and $\eta^{(1)}$ estimated from the data set in Fig. 2, using both the 2D (VTI) non-hyperbolic moveout equation in the $[x_2, x_3]$ plane (circles) and our 3D (full-azimuth) algorithm based on (9) (triangles). For each method, the inversion was performed for 100 randomly chosen starting models. The maximum offset-to-depth ratio is equal to (a) two, (b) three and (c) four. The cross marks the true model parameters.

Layered anisotropic media

Although (9) is designed for a single orthorhombic layer, we expect it to remain adequate for layered media with a uniform orientation of the vertical symmetry planes. If the medium above the reflector is multilayered, the moveout coefficients become effective quantities that incorporate the influence of both anisotropy and vertical heterogeneity. For example, the effective NMO ellipse can be found from the Dix-type averaging of the interval ellipses as described by Grechka *et al.* (1999).

The averaging equation for the interval quartic coefficients A_4 is more complicated and, in principle, can be obtained from the exact expression for A_4 presented by Pech *et al.* (2003). Al-Dajani and Tsvankin (1998), however, showed that if azimuthal anisotropy is not severe, a close approximation for A_4 is provided by averaging the interval quartic coefficients for each azimuth using the VTI equations of Tsvankin and Thomsen (1994) and Tsvankin (2005). Such an averaging operation results in the effective η parameter that has the same azimuthal dependence as that in (11) for a single orthorhombic layer.

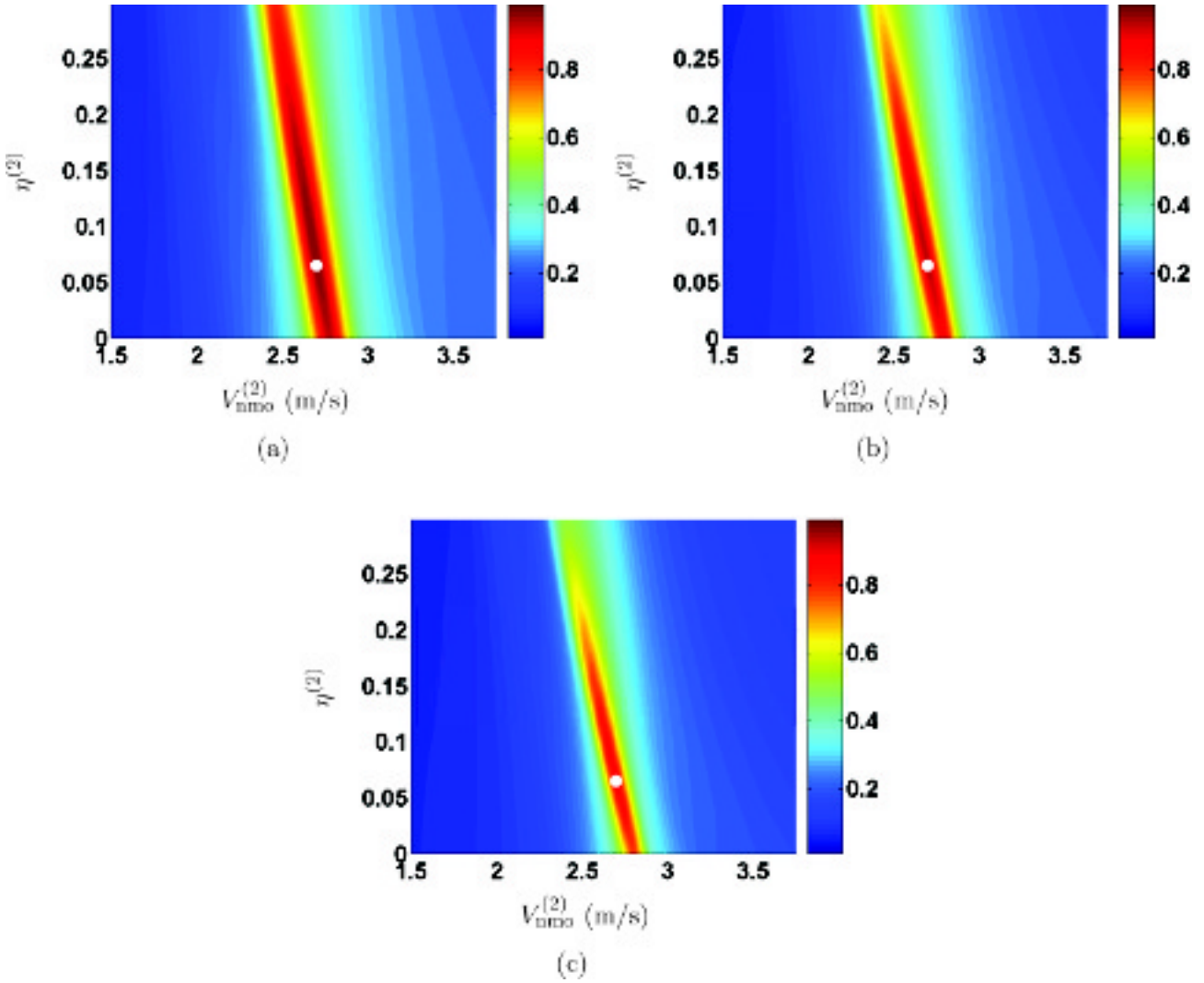

Figure 4 Semblance scans over $V^{(2)}_{\rm nmo}$ and $\eta^{(2)}$ computed from (9) for the following maximum offset-to-depth ratios: (a) $x/z = 2$, (b) $x/z = 2.5$, (c) $x/z = 3$. The model is the same as that in Fig. 2; the parameters φ, $V^{(1)}_{\rm nmo}$, $\eta^{(1)}$ and $\eta^{(3)}$ are fixed at the correct values. The white dots here and in following figures correspond to the true model.

The scope of the analysis below is limited to evaluating the accuracy of (9) with the best-fit effective moveout coefficients. The model in Fig. 7 includes an orthorhombic layer overlain by a VTI layer of equal thickness. Because of the smaller contribution of the azimuthally anisotropic layer to the total traveltime in this model, the resolution of the symmetry-plane azimuth φ is lower than that for a homogeneous orthorhombic medium. The error in φ, which in this case may be caused by a relatively small amount of noise, propagates into the rest of the moveout parameters, which, as discussed above, represent average values for the two layers. In general, the accuracy in estimating the symmetry-plane orientation depends on the relative thickness (i.e. on the ratio of the thickness and depth) of the azimuthally anisotropic layer.

Next, the inversion algorithm is applied to a two-layer orthorhombic model with misaligned symmetry planes (Fig. 8a,b) to evaluate the magnitude of the traveltime errors and study the relationship between the recovered value of the azimuth φ and the orientations of the symmetry planes in both layers. The 'true' value of φ, marked by the white dot in Fig. 8(a,b), is computed from the interval parameters of each layer by using the VTI averaging equations for η (Tsvankin 2005) at each azimuth. This averaging produces an azimuthally varying effective η function, whose principal direction is used to evaluate φ.

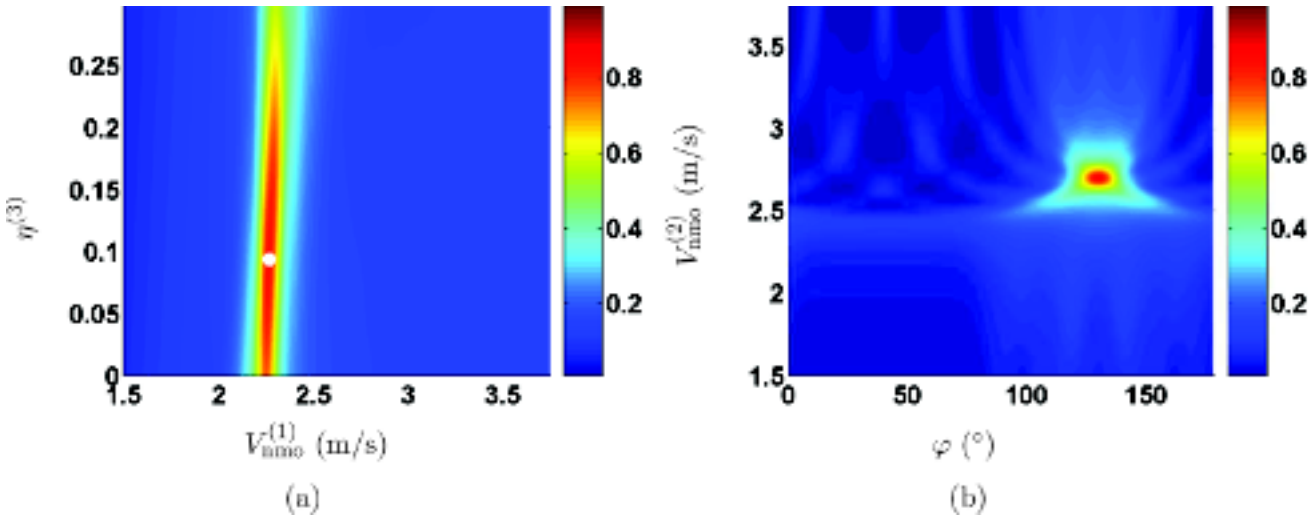

Figure 5 Semblance scans over (a) $\eta^{(3)}$ and $V_{\mathrm{nmo}}^{(1)}$, and (b) φ and $V_{\mathrm{nmo}}^{(2)}$, for the model in Fig. 2. For each scan, the other four parameters are fixed at the correct values; the maximum offset-to-depth ratio is three.

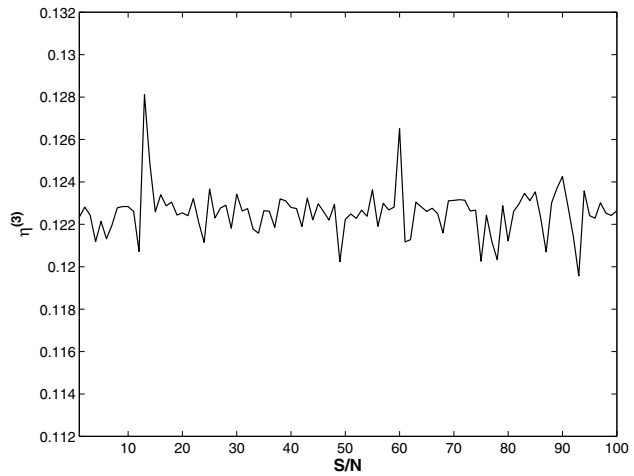

Figure 6 Inverted values of $\eta^{(3)}$ for variable signal-to-noise ratio. The synthetic data for the model in Fig. 2 were contaminated by Gaussian noise.

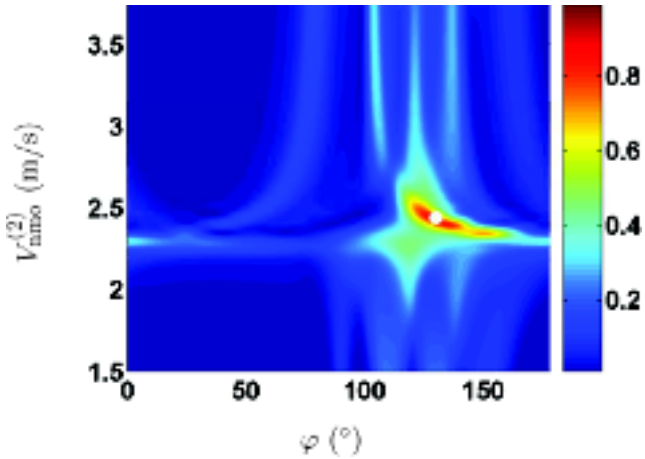

Figure 7 Semblance scans for the reflection from the bottom of a model composed of two layers with equal thickness. The orthorhombic layer from Fig. 2 is overlain by a VTI layer with $V_{\mathrm{nmo}} = 2158$ m/s and $\eta = 0.196$.

The value of φ estimated by our algorithm with the original equation (11) for $\eta(\alpha)$ (Fig. 8a) corresponds to a direction that is somewhat closer to the $[x_1, x_3]$ symmetry plane in the top layer. This best-fit value for φ deviates from the value predicted from the function $\eta(\alpha)$ (white dot) by approximately 15°, which indicates that the NMO ellipse and the azimuthally varying parameter η for this model have different principal axes.

Because this misalignment is ignored in (11), the semblance value for the best-fit model (0.69) is lower than the semblances obtained for a single layer and for the VTI/orthorhombic model. Although the reduced semblance indicates that the traveltimes computed from (9) deviate from the exact values, the magnitude of the traveltime residuals is limited by 1% (Fig. 9a).

As discussed above, to account for the influence of misaligned symmetry planes, we decouple the function $\eta(\alpha)$ from the NMO ellipse by replacing (11) for $\eta(\alpha)$ by (12). This modification helps to increase the value of semblance by about 20% (Fig. 8b) because the moveout equation now provides a closer fit to the exact traveltimes (Fig. 9b). Figure 8(b) shows that the azimuth φ_1 that corresponds to the maximum semblance

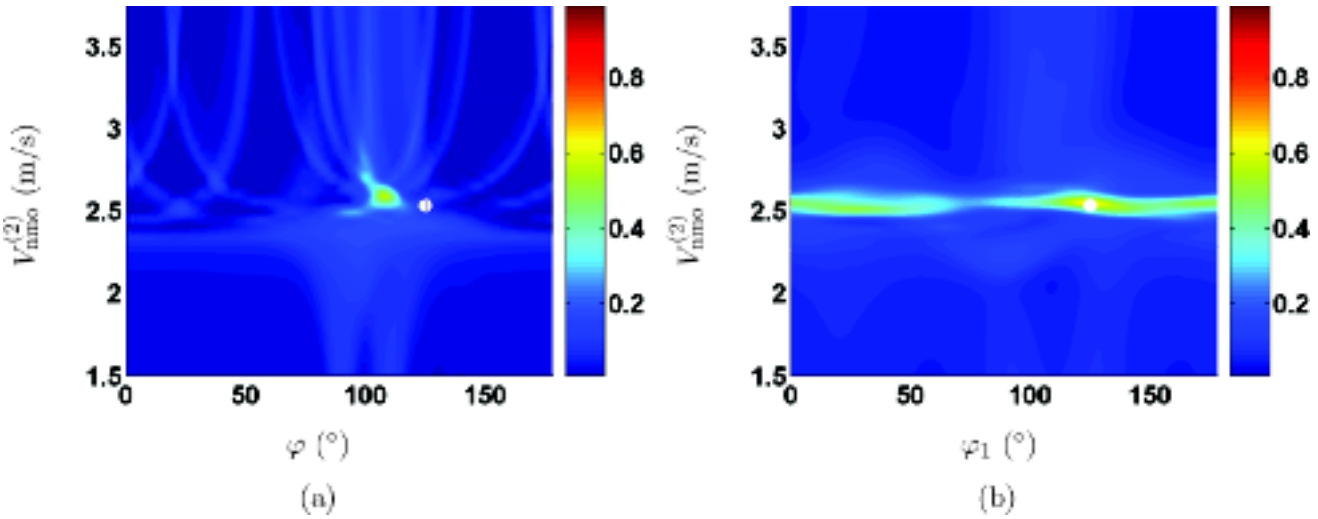

Figure 8 Semblance scans for the bottom reflection ($x/z = 3$) of a model, analogous to the one in Fig. 7, in which constituent layers are both orthorhombic. The orthorhombic layer from Fig. 2 is now overlain by an (a,b) orthorhombic layer with a different orientation of the symmetry planes ($\varphi = 90°$) and the parameters: $V^{(1)}_{\rm nmo} = 2156$ m/s, $V^{(2)}_{\rm nmo} = 2534$ m/s, $\eta^{(1)} = 0.398$, $\eta^{(2)} = 0.211$ and $\eta^{(3)} = 0.193$. The parameter estimation was performed using (a) equation (11) and (b) equation (12).

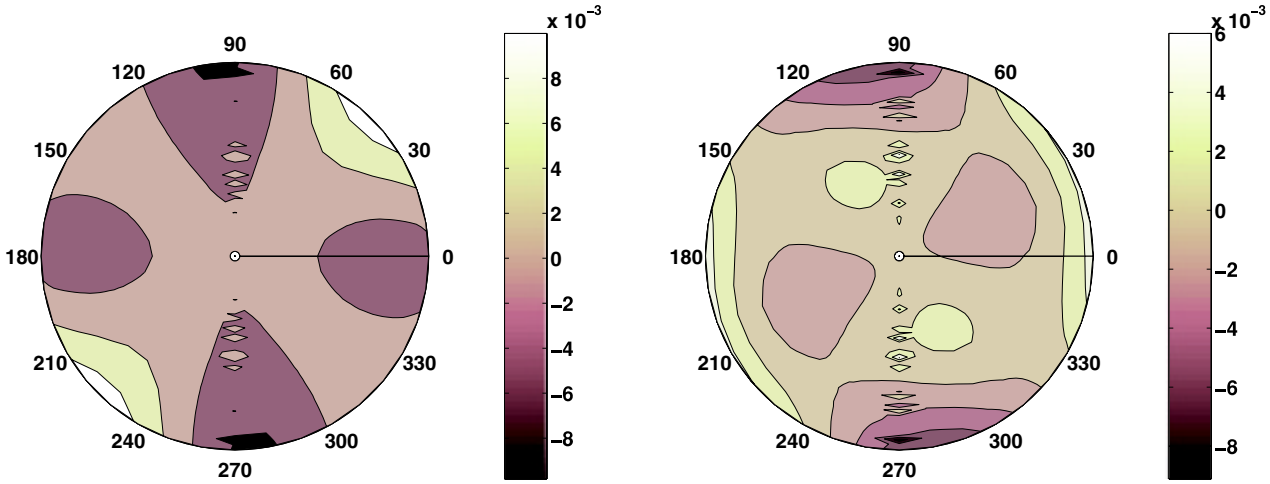

Figure 9 Azimuthally varying traveltime residuals for the model of two orthorhombic layers with misaligned symmetry planes (Fig. 8a). The residuals represent the differences between the ray-traced traveltimes computed for the true model and for the best-fit model obtained from the non-hyperbolic moveout inversion based on: (a) equation (11) (b) equation (12). The maximum offset-to-depth ratio is 2.5.

value is practically coincident with the theoretical prediction. However, φ_1 is not as well resolved as the azimuth φ responsible for the NMO ellipse, since φ_1 influences only the non-hyperbolic portion of the moveout curve. In general, the effective value of φ_1 is determined by the relative thicknesses, symmetry-plane orientations, and moveout parameters of the constituent layers.

FIELD-DATA EXAMPLE

We applied the moveout inversion algorithm to wide-azimuth P-wave data acquired at the Weyburn Field, located in the Williston Basin in Canada. This multicomponent data set was processed and interpreted by the Reservoir Characterization Project at the Colorado School of Mines with the main goal

of dynamic monitoring of the CO_2 flood in the fractured reservoir (only the base survey is used here). Jenner (2001) identified the presence of laterally varying azimuthal anisotropy at the reservoir level by computing the interval P-wave NMO ellipses and performing azimuthal AVO (amplitude variation with offset) analysis. He found the azimuthal dependence of the P-wave signatures in the overburden to be much less pronounced; his conclusions generally agree with the VSP-inversion results of Adam, van Wijk and Davis (2003).

The most reliable indicator of azimuthal anisotropy, however, is shear-wave splitting at near-vertical incidence, which was studied at the Weyburn Field by Cardona (2002). Comparison of the S-wave polarization directions with the orientation of the NMO ellipse allowed him to discriminate between different anisotropic symmetries at the reservoir level. According to Cardona's (2002) results, the magnitude of shear-wave splitting in the overburden is non-negligible, which probably indicates that most of the section is permeated by natural fractures.

The non-hyperbolic moveout inversion could potentially contribute to the seismic characterization of the reservoir by identifying the principal azimuthal directions of the quartic moveout coefficient and estimating the parameters $\eta^{(1,2,3)}$. As discussed above, if the azimuths of the symmetry planes above the reflector vary with depth, the principal directions of A_4 may deviate from the axes of the NMO ellipse. Another possible reason for such misalignment of the quadratic and quartic moveout coefficients is the presence of low anisotropic symmetries (i.e. monoclinic or lower) in the overburden. Therefore, the azimuthal variation of non-hyperbolic moveout could be used to verify the analysis of the anisotropic symmetries presented by Cardona (2002). Also, the parameters $\eta^{(1,2,3)}$ for fracture-induced orthorhombic media are sensitive to the orientations and compliances of the fractures and can provide valuable information for dynamic reservoir characterization (Bakulin *et al.* 2000; Pech and Tsvankin 2004).

The 3D non-hyperbolic moveout inversion [using equation (11) for $\eta(\alpha)$] was applied to P-waves collected into two 9×9 superbins, one of which is centred at CMP 10103 and the other at CMP 10829 (Fig. 10). The distribution of source-to-receiver azimuths and offsets for these superbins is shown in Fig. 10(a,b), while the NMO-corrected gathers in Fig. 10(c,d) confirm the presence of non-hyperbolic moveout and azimuthal traveltime variations. Unfortunately, the range of offsets acquired at the Weyburn Field is not sufficient for estimating the non-hyperbolic moveout term for reflections within or beneath the reservoir with acceptable accuracy. The maximum offset-to-depth ratio for the top of the reservoir horizon is only about 1.8, and the far-offset traces for that reflection are quite noisy. Also, the reservoir is thinner than half the dominant wavelength, which is below the vertical resolution of any traveltime method. In his estimation of the interval NMO ellipses, Jenner (2001) had to combine the reservoir with some underlying beds into a single coarse layer.

However, our methodology can be used to study the velocity field in the overburden, which consists of the four main horizons marked in Fig. 11 (the Mississippian Unconformity is close to the top of the reservoir). Clearly, anisotropy is quite substantial through most of the overburden, with the effective η values reaching 0.25 for the reflection from the deepest interface (the Mississippian Unconformity). The semblance scans in Fig. 12 demonstrate that the resolution in $\eta^{(2)}$ (and the other anellipticity parameters) decreases for the lower horizons because of the smaller offset-to-depth ratio. The relatively large uncertainty in $\eta^{(2)}$ for the Lower Vanguard reflection (Fig. 12c) is also caused by the high level of noise at far offsets. In principle, the error bars for the η values in Fig. 11 can be inferred from the size of the semblance contours in Fig. 12.

In contrast to the anellipticity parameters, the symmetry-plane azimuth φ is not well-constrained even for the shallow horizons (Fig. 13), which probably results from a relatively small magnitude of azimuthal anisotropy. The weak variation of φ with depth and the good accuracy provided by (11) exclude another possible reason for the instability in estimating φ, i.e. misaligned symmetry planes in the overburden layers. To verify whether it is possible to fit the data without taking azimuthal anisotropy into account, we ran the inversion algorithm for VTI media by setting $V^{(1)}_{\rm nmo} = V^{(2)}_{\rm nmo}$, $\eta^{(1)} = \eta^{(2)}$ and $\eta^{(3)} = 0$. The semblance values for the best-fit VTI model were on average 10% smaller than those for orthorhombic media, with the exception only of the Lower Vanguard reflection at CMP 10103 (for that event the reduction was only 5%). Since a 10% gain in semblance is not negligible (e.g. Grechka and Tsvankin 1999a), accounting for the azimuthal variation of reflection moveout does provide a better fit to the data.

Another indication of the influence of azimuthal anisotropy on reflection moveout is the consistency of the estimated symmetry-plane azimuth φ for all four reflection events at a fixed CMP location. If the non-hyperbolic moveout had no azimuthal signature, we would expect inverted values of φ to vary significantly from one event to another. Although the values of φ differ for CMP 10103 and CMP 10829, both estimated azimuths are close to the directions of the off-trend fracture sets identified from borehole data (Fig. 14).

The interpretation of the estimated anellipticity parameters is not straightforward because they represent effective values

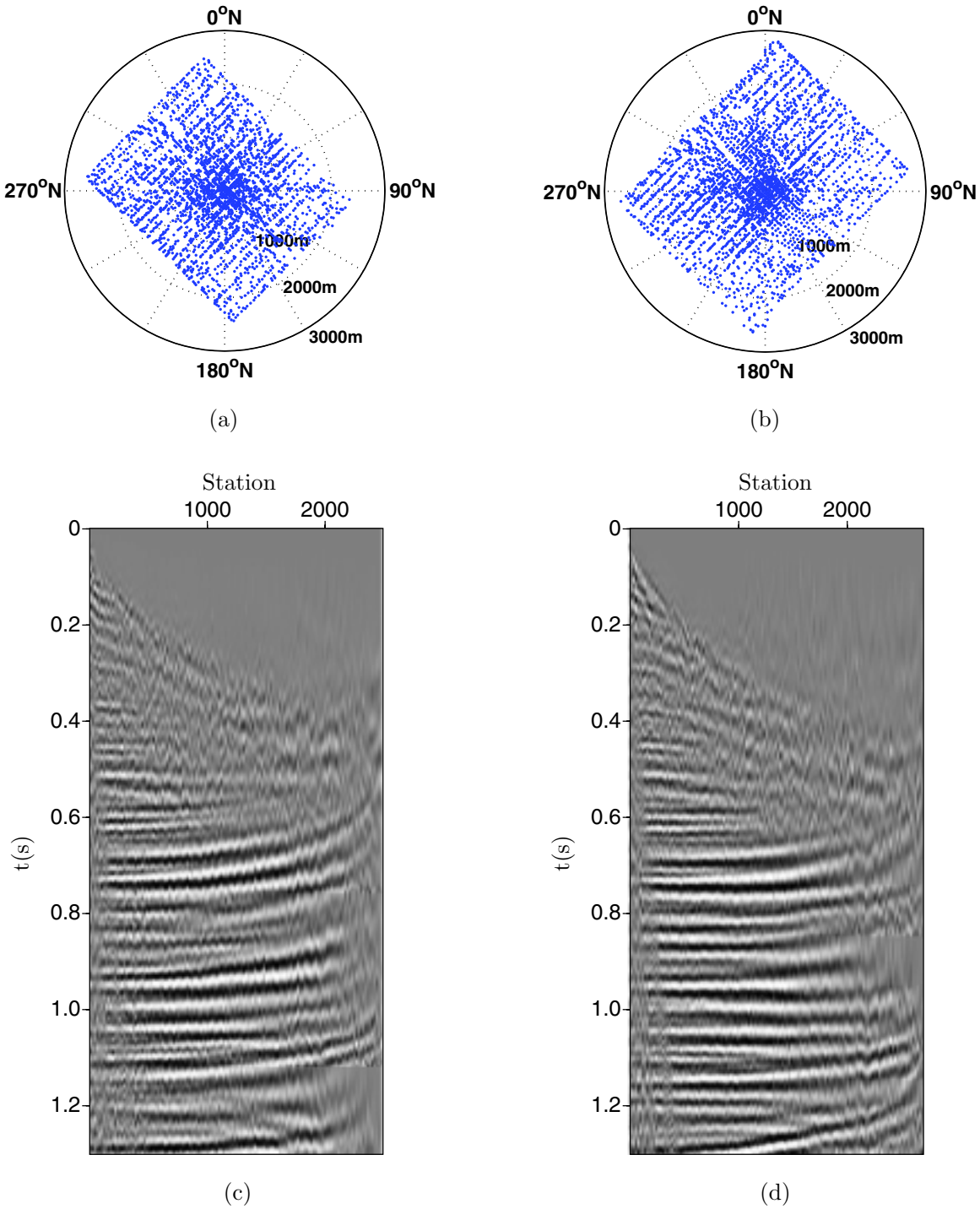

Figure 10 Source-to-receiver azimuth and offset coverage for the superbins centred at CMPs (a) 10103 and (b) 10829. Each point in these polar plots marks a source–receiver pair; the polar angle corresponds to the source-to-receiver azimuth in degrees from the north (see the numbers on the perimeter), whereas the radius is the offset (in metres). Also shown are gathers for superbins (c) 10103 and (d) 10829 after a conventional hyperbolic NMO correction (the moveout velocities are estimated for offset-to-depth ratios of up to unity). The gathers are sorted by increasing offset and contain all azimuths and offsets, which are irregularly sampled [see plots (a) and (b)]. The 'jittery' character of the reflections suggests that the traveltimes vary with azimuth. The curvature of the NMO-corrected events at long offsets indicates the influence of non-hyperbolic moveout. The total fold is 2491 for superbin 10103 and 2702 for superbin 10829.

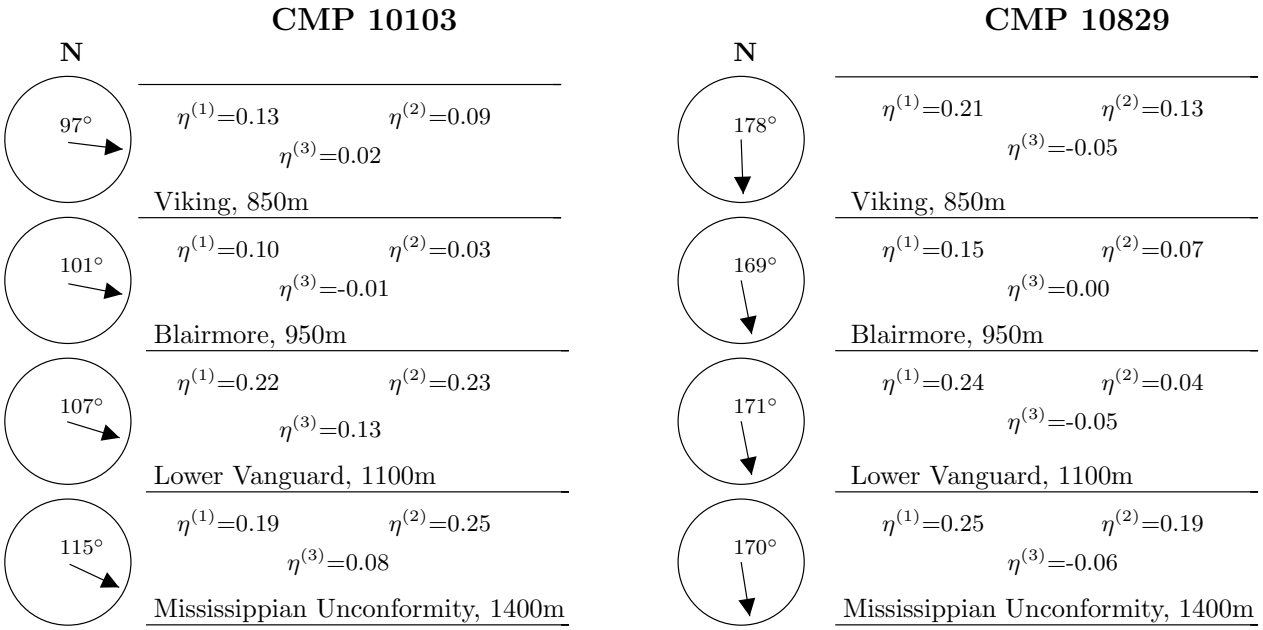

Figure 11 Inversion results for the reflections from (a) the Viking horizon, the maximum offset-to-depth ratio $x/z = 2.5$; (b) the Blairmore, $x/z = 2.0$; (c) the Lower Vanguard, $x/z = 1.9$; (d) the Mississippian Unconformity, $x/z = 1.8$. The arrows mark the estimated direction of the semi-major axis of the NMO ellipse; the number by each arrow is the azimuth of the axis with respect to the north. All η parameters are the effective values for a given reflection event.

for the stack of layers above the reflector. However, the substantial magnitude of $\eta^{(1)}$ and $\eta^{(2)}$ for the Viking reflection at CMP 10829 (Figs 11 and 12) imply that the upper part of the section is moderately anisotropic. Also, the large difference between $\eta^{(1)}$ and $\eta^{(2)}$ for the Viking is a clear sign of non-negligible azimuthal anisotropy. The decrease in the effective η parameters for the Blairmore reflection suggests that the interval between the Viking and Blairmore is weakly anisotropic.

The magnitude of non-hyperbolic moveout increases at the Lower Vanguard horizon, in particular for CMP 10103, which may be explained by stronger anisotropy beneath the Blairmore. The Lower Vanguard reflection, however, is not distinct at far offsets, and the semblance values for it are about 15% smaller than those for the other horizons. Finally, although $\eta^{(2)}$ at CMP 10829 increases for the Mississippian Unconformity, the uncertainty in the estimation of the anellipticity coefficients for this horizon render the inversion results unreliable. Also, the effective anellipticity parameters for the deeper horizons are influenced by the vertical heterogeneity (e.g. the velocity gradients) in the overburden.

The moveout-inversion results in Fig. 11 were successfully used by Xu and Tsvankin (2004) to correct the wide-azimuth, long-spread reflection from the reservoir for anisotropic geometrical spreading.

DISCUSSION AND CONCLUSIONS

Long-spread moveout of P-waves in orthorhombic media with a horizontal symmetry plane is governed by the azimuth φ of one of the vertical symmetry planes, the symmetry-plane NMO velocities $V^{(1)}_{\rm nmo}$ and $V^{(2)}_{\rm nmo}$, and the anellipticity parameters $\eta^{(1)}$, $\eta^{(2)}$ and $\eta^{(3)}$. Here, we apply a modified version of the non-hyperbolic moveout equation of Alkhalifah and Tsvankin (1995) to invert for these six parameters from wide-azimuth, long-offset data. The inversion algorithm is organized as a three-step procedure that starts with estimation of the NMO ellipse on conventional-length spreads using the method of Grechka and Tsvankin (1999a). After evaluating the azimuths of the symmetry planes and the velocities $V^{(1)}_{\rm nmo}$ and $V^{(2)}_{\rm nmo}$ from the NMO ellipse, we perform 2D inversion for the parameters $\eta^{(1)}$ and $\eta^{(2)}$ in the symmetry-plane directions. The obtained initial values of the moveout parameters are then used in a global semblance search that operates with data for all available offsets and azimuths.

Although our moveout equation is based on the analogy with VTI media, which is not strictly valid in off-symmetry directions, the inversion provides sufficiently accurate results even for models with strong azimuthal anisotropy. Since the azimuth φ and the velocities $V^{(1)}_{\rm nmo}$ and $V^{(2)}_{\rm nmo}$ define the NMO

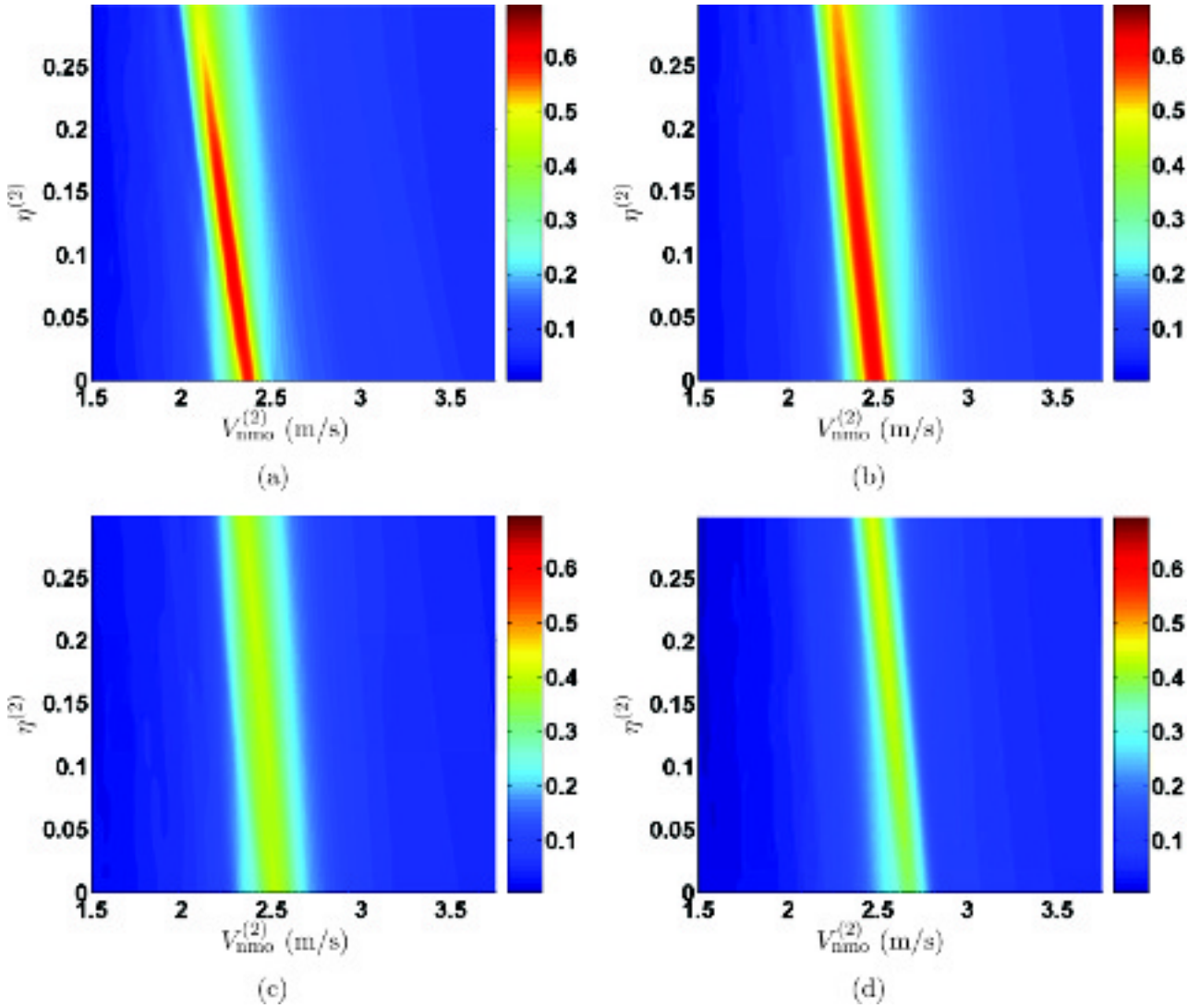

Figure 12 Semblance scans over $V_{\rm nmo}^{(2)}$ and $\eta^{(2)}$ at CMP 10103 for the reflections from (a) the Viking horizon, (b) the Blairmore, (c) the Lower Vanguard, (d) the Mississippian Unconformity.

ellipse, they are constrained better than the parameters $\eta^{(1)}$, $\eta^{(2)}$ and $\eta^{(3)}$, which make a significant contribution to the traveltimes only for large offset-to-depth ratios (e.g. x/z exceeding 1.5–2). As is the case for VTI media, estimation of the anellipticity parameters is hampered by the trade-offs between $V_{\rm nmo}^{(1)}$ and $\eta^{(1)}$ and between $V_{\rm nmo}^{(2)}$ and $\eta^{(2)}$ (Grechka and Tsvankin 1998b). These trade-offs can cause substantial uncertainties in $\eta^{(1)}$ and $\eta^{(2)}$ if the data are contaminated by correlated noise and the maximum ratio x/z is smaller than 2.5. Our 3D (full-azimuth) algorithm typically produces estimates of the parameters $\eta^{(1)}$ and $\eta^{(2)}$ with accuracy close to that of the 2D (VTI) inversion in the symmetry planes (for offset-to-depth ratios of up to three). The least-constrained model parameter is $\eta^{(3)}$ because it influences only long-spread moveout in off-symmetry directions.

The moveout equation used here gives a close approximation for P-wave non-hyperbolic moveout not just in homogeneous media, but also in layered azimuthally anisotropic models with a uniform direction of the vertical symmetry planes. The accuracy of estimating the symmetry-plane azimuth φ, however, is reduced if an orthorhombic layer is overlain by a relatively thick azimuthally isotropic (e.g. VTI) overburden.

If the orientation of the symmetry planes varies with depth, our moveout equation is less accurate and yields smaller semblance values because of the misalignment of the axes of the

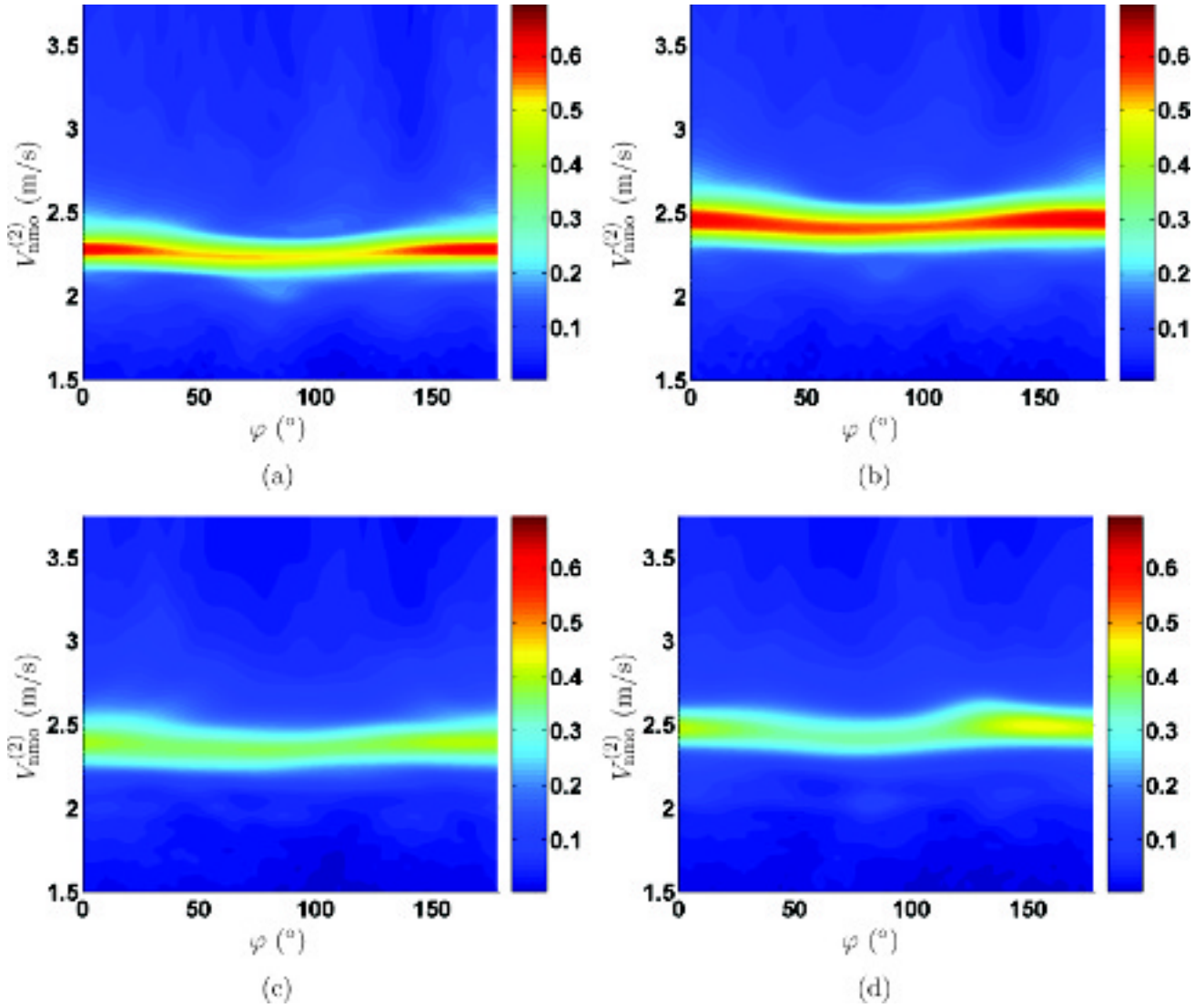

Figure 13 Semblance scans over $V^{(2)}_{\rm nmo}$ and φ at CMP 10103 for the reflections from (a) the Viking horizon, (b) the Blairmore, (c) the Lower Vanguard, (d) the Mississipian Unconformity. The azimuth φ is measured counterclockwise from the survey's x-axis, which points eastward.

NMO ellipse and the principal directions of the azimuthally varying effective parameter η. Moveout inversion for models without throughgoing vertical symmetry planes can be substantially improved by introducing an additional angle (φ_1) responsible for the azimuthal dependence of η.

Application of our methodology to wide-azimuth P-wave data acquired over a fractured reservoir at the Weyburn Field in Canada reveals a substantial magnitude of non-hyperbolic moveout and non-negligible azimuthal anisotropy in the overburden. Although the deeper horizons are known to be azimuthally anisotropic as well, the offsets were not large enough to estimate the anellipticity parameters at the reservoir level. Because the reflection moveout seems to be largely controlled by polar anisotropy (i.e. by vertical transverse isotropy), the resolution of the symmetry-plane orientation is relatively low. Nevertheless, taking azimuthal anisotropy into account increases the semblance for most events by about 10% and produces consistent values of the azimuth φ for all four horizons used in the analysis.

The symmetry-plane directions estimated from the non-hyperbolic moveout analysis closely match the azimuths of the off-trend fracture sets in the area. Also, our conclusion that the magnitude of azimuthal anisotropy is significant mostly in the shallow part of the section (above the Lower Vanguard horizon) is in agreement with the shear-wave splitting analysis of Cardona (2002). A more detailed interpretation of the

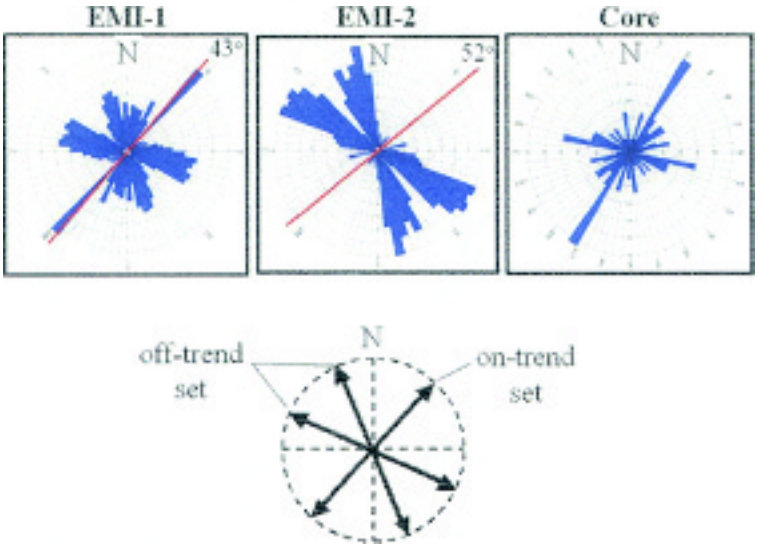

Figure 14 Fracture counts for different fracture azimuths from well-log images and core analysis (after Cardona 2002). Well EMI1 is located close to superbin CMP 10103. The estimated symmetry-plane azimuths for CMP 10103 and CMP 10829 roughly match the directions of the off-trend fracture sets.

inversion results may be attempted in the future by applying layer stripping to the effective values of the anellipticity parameters obtained from non-hyperbolic moveout.

It should be emphasized that while fracture characterization and lithology discrimination require the interval anellipticity parameters for the horizon of interest, the effective values of $\eta^{(1,2,3)}$ and $V_{\rm nmo}^{(1,2)}$ produced by our algorithm are sufficient for several important applications in seismic processing. First, our method makes it possible to accurately flatten wide-azimuth, long-spread CMP gathers prior to stacking or azimuthal AVO analysis. Second, as long as (9) provides a good approximation for long-spread reflection traveltimes, the effective homogeneous orthorhombic model defined by the best-fit moveout parameters can be used for post-stack (and, possibly, pre-stack) time imaging of P-wave data. Third, Xu and Tsvankin (2004) developed a correction for geometrical spreading in layered orthorhombic media based on (9) with the effective moveout parameters estimated using our algorithm. They also used our field-data results to correct the wide-azimuth, long-spread reflection from the top of the reservoir at the Weyburn Field for anisotropic geometrical spreading.

ACKNOWLEDGEMENTS

We thank Edward Jenner (currently GX Technology), Tom Davis and Marty Terrell (currently Exxon Mobil) of the Reservoir Characterization Project at Colorado School of Mines (CSM) for providing the Weyburn Field data and discussing their interpretation results with us. I.V. is grateful to the Department of Geophysics of the University of São Paulo, Brazil, for assistance with his visit to the Center for Wave Phenomena (CWP) at CSM in 2003. Many thanks to Alison Malcolm and Xiaoxia Xu (both CSM) for their help with many aspects of this project; X. Xu also provided Fig. 9. This work was supported by the Consortium Project on Seismic Inverse Methods for Complex Structures at CWP and by the Chemical Sciences, Geosciences and Biosciences Division, Office of Basic Energy Sciences, U.S. Department of Energy.

REFERENCES

Adam L., van Wijk K. and Davis T. 2003. Multi-level 3D VSP travel time inversion in VTI media, Weyburn field, Canada. 73rd SEG Meeting, Dallas, USA, Expanded Abstracts, 753–756.

Al-Dajani A. and Tsvankin I. 1998. Non-hyperbolic reflection moveout for horizontal transverse isotropy. *Geophysics* **63**, 1738–1753.

Al-Dajani A., Tsvankin I. and Toksöz M.N. 1998. Non-hyperbolic reflection moveout for azimuthally anisotropic media. 68th SEG Meeting, New Orleans, USA, Expanded Abstracts, 1479–1482.

Alkhalifah T. 1997. Velocity analysis using non-hyperbolic moveout in transversely isotropic media. *Geophysics* **62**, 1839–1854.

Alkhalifah T. and Tsvankin I. 1995. Velocity analysis for transversely isotropic media. *Geophysics* **60**, 1550–1566.

van der Baan M. 2004. Processing of anisotropic data in the $\tau - p$ domain: I – Geometric spreading and moveout corrections. *Geophysics* **69**, 719–730.

Bakulin A., Grechka V. and Tsvankin I. 2000. Estimation of fracture parameters from reflection seismic data–Part II: Fractured models with orthorhombic symmetry. *Geophysics* **65**, 1803–1817.

Cardona R. 2002. *Fluid substitution theories and multicomponent seismic characterization of fractured reservoirs*. PhD Thesis, Colorado School of Mines.

Douma H. and Calvert A. 2006. Non-hyperbolic moveout analysis in VTI media using rational interpolation. *Geophysics* **71**, D59–D71.

Fomel S. 2004. On anelliptic approximations for qP velocities in VTI media. *Geophysical Prospecting* **52**, 247–259.
Gajewski D. and Pšenčík I. 1987. Computation of high frequency seismic wavefields in 3-D laterally inhomogeneous anisotropic media. *Geophysical Journal of the Royal Astronomical Society* **91**, 383–412.
Grechka V., Pech A. and Tsvankin I. 2002. Multicomponent stacking-velocity tomography for transversely isotropic media. *Geophysics* **67**, 1564–1574.
Grechka V. and Tsvankin I. 1998a. 3-D description of normal moveout in anisotropic inhomogeneous media. *Geophysics* **63**, 1079–1092.
Grechka V. and Tsvankin I. 1998b. Feasibility of non-hyperbolic moveout inversion in transversely isotropic media. *Geophysics* **63**, 957–969.
Grechka V. and Tsvankin I. 1999a. 3-D moveout inversion in azimuthally anisotropic media with lateral velocity variation: Theory and a case study. *Geophysics* **64**, 1202–1218.
Grechka V. and Tsvankin I. 1999b. 3-D moveout velocity analysis and parameter estimation for orthorhombic media. *Geophysics* **64**, 820–837.
Grechka V., Tsvankin I. and Cohen J.K. 1999. Generalized Dix equation and analytic treatment of normal-moveout velocity for anisotropic media. *Geophysical Prospecting* **47**, 117–148.
Jenner E. 2001. *Azimuthal anisotropy of 3-D compressional wave seismic data, Weyburn Field, Saskatchewan, Canada*. PhD. Thesis, Colorado School of Mines.
Pech A. and Tsvankin I. 2004. Quartic moveout coefficient for a dipping azimuthally anisotropic layer. *Geophysics* **69**, 699–707.
Pech A., Tsvankin I. and Grechka V. 2003. Quartic moveout coefficient: 3D description and application to tilted TI media. *Geophysics* **68**, 1600–1610.
Press W.H., Teukolsky S.A., Vetterling W.T. and Flannery B.P. 1987. *Numerical Recipes in C*. Cambridge University press.
Sayers C.M. and Ebrom D.A. 1997. Seismic traveltime analysis for azimuthally anisotropic media: Theory and experiment. *Geophysics* **36**, 1570–1582.
Schoenberg M. and Helbig K. 1997. Orthorhombic media: Modeling elastic wave behavior in a vertically fractured earth. *Geophysics* **62**, 1954–1974.
Stovas A. and Ursin B. 2004. New travel-time approximations for a transversely anisotropic medium. *Journal of Geophysical Engineering* **1**, 128–133.
Thomsen L. 1986. Weak elastic anisotropy. *Geophysics* **51**, 1954–1966.
Toldi J., Alkhalifah T., Berthet P., Arnaud J., Williamson P. and Conche B. 1999. Case study of estimation of anisotropy. *The Leading Edge* **18**, 588–594.
Tsvankin I. 1997. Anisotropic parameters and P-wave velocity for orthorhombic media. *Geophysics* **62**, 1292–1309.
Tsvankin I. 2005. *Seismic Signatures and Analysis of Reflection Data in Anisotropic Media* (2nd edition). Elsevier Science Publishing Co.
Tsvankin I. and Thomsen L. 1994. Non-hyperbolic reflection moveout in anisotropic media. *Geophysics* **59**, 1290–1304.
Xu X. and Tsvankin I. 2004. Geometrical-spreading correction for P-waves in layered azimuthally anisotropic media. 74th SEG Meeting, Denver, USA, Expanded Abstracts, 111–114.
Xu X., Tsvankin I. and Pech A. 2005. Geometrical spreading of P-waves in horizontally layered, azimuthally anisotropic media. *Geophysics* **70**, D43–D53.

APPENDIX

Notation for orthorhombic media

Seismic inversion and processing for orthorhombic media (see Fig. 1) can be facilitated by combining the stiffness coefficients in a way that simplifies analytic description of seismic signatures. The identical form of the Christoffel equation in the symmetry planes of orthorhombic and TI media allowed Tsvankin (1997) to introduce a notation based on the same principle as Thomsen (1986) parameters for vertical transverse isotropy. This notation includes two reference velocities (the vertical velocities of the P-wave and one of the split S-waves) and seven dimensionless anisotropic parameters defined in the symmetry planes by analogy with the VTI coefficients ϵ, δ and γ:

- V_{P0} – the P-wave vertical velocity:

$$V_{P0} \equiv \sqrt{\frac{c_{33}}{\rho}} \quad (\rho \text{ is the density}). \tag{A1}$$

- V_{S0} – the vertical velocity of the S-wave polarized in the x_1-direction:

$$V_{S0} \equiv \sqrt{\frac{c_{55}}{\rho}}. \tag{A2}$$

- $\epsilon^{(2)}$ – the VTI parameter ϵ in the $[x_1, x_3]$ symmetry plane (the superscript 2 refers to the orthogonal axis x_2):

$$\epsilon^{(2)} \equiv \frac{c_{11} - c_{33}}{2\,c_{33}}. \tag{A3}$$

- $\delta^{(2)}$ – the VTI parameter δ in the $[x_1, x_3]$ plane:

$$\delta^{(2)} \equiv \frac{(c_{13} + c_{55})^2 - (c_{33} - c_{55})^2}{2\,c_{33}\,(c_{33} - c_{55})}. \tag{A4}$$

- $\gamma^{(2)}$ – the VTI parameter γ in the $[x_1, x_3]$ plane:

$$\gamma^{(2)} \equiv \frac{c_{66} - c_{44}}{2\,c_{44}}. \tag{A5}$$

- $\epsilon^{(1)}$ – the VTI parameter ϵ in the $[x_2, x_3]$ symmetry plane:

$$\epsilon^{(1)} \equiv \frac{c_{22} - c_{33}}{2\,c_{33}}. \tag{A6}$$

- $\delta^{(1)}$ – the VTI parameter δ in the $[x_2, x_3]$ plane:

$$\delta^{(1)} \equiv \frac{(c_{23} + c_{44})^2 - (c_{33} - c_{44})^2}{2\,c_{33}\,(c_{33} - c_{44})}. \tag{A7}$$

- $\gamma^{(1)}$ – the VTI parameter γ in the $[x_2, x_3]$ plane:

$$\gamma^{(1)} \equiv \frac{c_{66} - c_{55}}{2\,c_{55}}. \tag{A8}$$

- $\delta^{(3)}$ – the VTI parameter δ in the $[x_1, x_2]$ symmetry plane (x_1 plays the role of the symmetry axis):

$$\delta^{(3)} \equiv \frac{(c_{12}+c_{66})^2-(c_{11}-c_{66})^2}{2\,c_{11}\,(c_{11}-c_{66})}\,. \tag{A9}$$

Tsvankin (1997, 2001) showed that this notation provides a convenient description of phase and NMO velocities, reflection coefficients, and other signatures both within and outside the symmetry planes. Also, P-wave phase and group velocity depends on just six parameters: (V_{P0}, $\epsilon^{(1)}$, $\delta^{(1)}$, $\epsilon^{(2)}$, $\delta^{(2)}$ and $\delta^{(3)}$), and the orientation of the symmetry planes, rather than on nine coefficients in the conventional (c_{ij}) notation.

However, only five combinations of these six parameters (for fixed symmetry-plane azimuths) govern P-wave *time-domain* signatures in homogeneous orthorhombic media. Reflection moveout and time-imaging operators for P-waves are controlled by the two symmetry-plane NMO velocities from horizontal reflectors and the following three anellipticity parameters, defined by analogy to the coefficient η in VTI media (Grechka and Tsvankin 1999b):

$$\eta^{(1)} \equiv \frac{\epsilon^{(1)}-\delta^{(1)}}{1+2\delta^{(1)}}\,, \tag{A10}$$

$$\eta^{(2)} \equiv \frac{\epsilon^{(2)}-\delta^{(2)}}{1+2\delta^{(2)}}\,, \tag{A11}$$

$$\eta^{(3)} \equiv \frac{\epsilon^{(1)}-\epsilon^{(2)}-\delta^{(3)}(1+2\epsilon^{(2)})}{(1+2\delta^{(3)})(1+2\epsilon^{(2)})}\,. \tag{A12}$$